Article

Cement Raw Material Reserve Calculation—Geological Sections vs. Structural Maps Approaches, Case Study from Southern Croatia

Nikolina Bralić [1,*] and **Tomislav Malvić** [2]

1   Cemex Hrvatska d.d, F. Tuđmana 45, HR–21212 Kaštel Sućurac, Croatia
2   Faculty of Mining, Geology and Petroleum Engineering, University of Zagreb, Pierottijeva 6, HR–10000 Zagreb, Croatia
*   Correspondence: nikolina.bralic@cemex.com

Abstract: This study aims to compare two approaches for the reserve calculation of cement raw material by geological sections and structural maps. The first is legally based, and its accuracy is approved by periodical calculation of the exploited material on site. In this research, it was crucial to determine deviation in the calculation approach, i.e., geological section volume calculation versus the volume obtained as a software solution estimated as a number of cells between two structural maps, i.e., maps interpolated at the top and bottom of the analysed lithological unit. Due to complex mineralogy, raw cement needs different energy consumption that directly affects the procedure of cement production, e.g., increases in air pollution through CO_2 emissions. The research area was the exploitation field "St. Juraj–St. Kajo," situated near the town of Split, region of Dalmatia, Southern Croatia. In the deposit, there are seven different lithological units, and all were technologically divided based on their chemical compounds. The lithology included dominantly marl and sandstone with occasional alternations of the conglomerate. Although in the geological sense it is considered a single unit, it partially contains interlayers in the form of lenses such as limy (calcitic) marl, clacisiltite (clayey limestone), and clayey marl. Generally, the knowledge of interlayers' existence is more important than their exact quantity because it affects expectations of a nonuniform material's technological quality at the location. For the purpose of the analysed lithological unit calculation, the volumes of the interlayers within were determined as well. Using geological sections for volume calculation is based on the calculation of the block volume (V) between two parallel vertical sections (P_1, P_2), which is obtained as a product of the mean areas (Paverage) of adjacent parallel sections (P_1, P_2) multiplied by the distance between them (d). Structural maps represent the calculation of the volume of the analysed object under a function f (x, y) defined by a double definite integral. Comparison of research results encourages the use of software solutions for the volume calculation of cement raw material volume in the future.

Keywords: reserve calculation; cement raw material; flysch; geological section; structural map; trapezoidal rule; Simpson's rule

1. Introduction

The reserve calculation is the primary basis for gaining insight into the volume and value of raw material deposits. It should be kept in mind that the calculation of reserves is mainly a geological rather than a mathematical task [1], e.g., data generally have an equivocal pattern until a meaningful pattern can be developed by geological and statistical interpretation [2]. The number of exploration boreholes is a key control factor for calculating the reserve, which gives one of the most reliable images of subsurface lithology [3]. The volume calculations of the various reservoirs/deposits are partly similar, whatever the types of reserves are observed. For example, in the case of hydrocarbons, some fundamental uncertainties are numerically described in [4]. Within shallow hydrogeological

systems, pore volumes as a basis for volume calculation can be numerically expressed by simulations [5]. In a cement plant, a complex technological process starts with the excavation of the raw material from the lithological units in the deposit. A complex mineral composition is used as the main input material in cement production, leading to different energy consumption in their processing (e.g., [6]), directly impacting the environment with different pollutants, like CO_2 emissions. Approximately 40% of cement plant CO_2 emissions are from the burning of fossil fuel to operate the rotary kiln, 50% due to the manufacturing process (the calcination process), and the remaining 10% are accounted for by indirect CO_2 emissions relating to transportation of the product and front-end production processes [7–9].

As the case study for this analysis is taken, the "Sv. Kajo" and "Sv. Juraj" cement plants in Solin and Kaštel Sućurac (towns near Split as urban agglomerate), owned by Cemex Croatia, part of the Cemex Group, one of the world's largest manufacturers of construction materials based in Mexico and present in more than 50 countries worldwide. "Sv. Kajo" was produced in 1908, and "Sv. Juraj" from 1912 until today. Technologically, the Eocene flysch is considered raw cement material (although only marl was used as raw material until 1970) with different qualities in different lithological units. Shallow, and sometimes surface-level exposure, hydrogeological researching of entire flysch sequences was important and showed that the Eocene clastics were mostly not subdued to karstification, despite to the regional Dinaric karst zone (e.g., [10]). Consequently, the flysch represents the complete or partial barrier to subsurface streams, creating the springs at the contact of the flysch and limestones. One of the most prominent is the spring of the Jadro River, which is the main source of potable water for the Split urban area and shallow ground water levels.

As a numerical procedure, the reserve calculation can be sensitive regarding numerous variables like mineralogy, clearness of marker beds, selected gridding methods, and cell sizes (e.g., [3]). Such calculations can be done with different mapping and geometrical methods, such as isopachs or structural maps, the polygonal approach, and related volumes obtained with Simpson or trapezoid equations (e.g., [2,8]). The availability of quick and powerful computing systems led to the development and acceptance of different tools in order to optimize exploitation scheduling [11]. The accuracy of the reserve calculation is also evaluated as the material is periodically exploited, which obtains data accumulation. Consequently, the reserve calculations become more reliable unless there is an unexpected change in geologic conditions [2].

Such calculations are developed in different types of ore deposits for estimations of grades, volumes, stockpiles qualities, blending processes, etc. Ref. [12] presented linear programming to obtain the optimum blending operations in mining sites, which also included estimating ore reserves with a triangular method. A similar approach of linear programming was applied [13]. The single stockpile is used for keeping low-grade material based on the availability of processing capacity and for possible future processing. Deterministic models are used to calculate the average grade for gold and iron as two case studies. Ref. [14] presented reserve's calculation methods in extremely skewed grade values of gold deposit, using five machine learning algorithms. The ranking shows that the Gaussian Process Regression with logarithmic normalization is the most efficient method for estimating gold grade, far outperforming the Ordinary and Indicator Kriging techniques. The application of the Kriging in ore calculation is also shown by [15], where the Ordinary Kriging was used for mapping the accompanying elements (Co, Ni, Pb, and V) in the primary mineralisation (Cu). It was found that the standard kriging error in accompanying elements locally is 2–5 times larger than in data of the main element, and reliable assessment is possible only with additional sampling. Assessment of uncertainties in the cement raw material deposits in Southern Vietnam has been shown using hierarchical simulations where rock types and chemical grades are emulated. Additionally, Ref. [16] concluded that such techniques can be applied for reaching satisfactory raw material grades when mixing several lithologies in the material processing. In addition, Ref. [17] showed the application of the Plurigausssian simulations for the prediction of lithology in cement

raw material deposits, including limestones, marl, and sandstone in the Adana Cement Factory (Turkey). The results showed localised lithotypes schemes as base for successful processing of excavated material as a mix of several lithological units. The study presented in [18] used geostatistical and neural approaches to estimate the lime saturation factor in clinker, i.e., the quality of cement. The adaptive neural algorithm showed better results in distribution prediction of the mentioned factor, i.e., connection with the geology of the deposit.

Due to the points above, we considered it crucial to determine the appropriate reserve calculation approach for the presented largest Croatian cement raw material mine and processing site, i.e., check the previously used geological section calculation versus the volume estimated as a number of cells between two structural maps, i.e., maps interpolated at the top and bottom of the lithological unit. We also tried to take it a step further and considered the smallest recognised layers inside the Eocene flysch sequence as mining targets. For the sake of accuracy, the interlayers observed in lithological unit 1 are considered, delimiting them on the sections as well as on the separate structural maps.

2. Geological Settings

Geological settings include the regional geology, meaning the corresponding lithostratigraphy and the lithological, mineralogical, and chemical properties of seven lithological units described in the analysed area.

2.1. Regional Settings

The coastal parts of Croatia belong mostly to the Adriatic Carbonate Platform and are dominated by the SW-verging Dinaric fold belt. The stratigraphy is characterised by a thick carbonate succession ranging from Carboniferous to Miocene [19]. According to [20], there are four mega-sequences. From the oldest, they are: "*(1) a pre-platform succession ranging in age from Late Carboniferous (Middle Pennsylvanian: Moscovian) to Early Jurassic (Early Toarcia; Brušane and Baške Ostarije Formations); (2) an Early Jurassic to Late Cretaceous platform mega-sequence (Mali Alan Formation); (3) a Paleogene to Neogene post—platform mega-sequence (Raša Formation); and (4) a Neogene to Quaternary (Pliocene to Holocene) mega-sequence (Istra and Ivana Formations)*". Almost simultaneously [21] defined lithostratigraphic equivalent to the Istra and Ivana Formations described in the Northern Adriatic, i.e., in the Croatian part of the Po Depression. As the palaeogeography differed in the Dalmatia and the Northern Adriatic, in the south, the Neretva Channel Formation was introduced as the equivalent of the Ivana Formation, covering Neogene and Quaternary. The analysed area belongs to the Palaeogene (Eocene), i.e., lithosratigraphically to the Raša Formation, when part of platform sediments had been uplifted [22] into the Dinaric orogeny mountains.

The research has been done in the exploitation field "St. Juraj–St. Kajo," situated near the town of Split, in the region of Middle Dalmatia, Southern Croatia. The raw material in the exploitation field, "St. Juraj–St. Kajo", was chronostratigraphically analysed according to significant lithological variation expressed through seven lithological units (after [23]), shown in Figure 1 [24,25]. Lithologically, the units differ the most in their texture and clay and limestone content. The analysed lithological unit 1 dominantly included marl and sandstone with lenses of conglomerates, covering the largest area of the exploitation field, and small interlayers of different lithological characteristics within.

In the flysch deposits (the Raša Formation), clastics are mostly in tectonic contact with the sedimentary rocks at the top and bottom. Additionally, in the northern part of the exploitation field, "St. Juraj–St. Kajo", flysch deposits are over-thrust by the older Mesozoic carbonate sedimentary rocks [26]. The flysch generically belongs to the tectonically active area in the past as well as today. The analysed area was affected by the collision between the Adriatic microplate and European Plate, i.e., strong deformation reflected in the Adriatic Carbonate Platform sediments. One of the results is the flysch incorporated into different carbonate complexes [27]. The flysch was deposited after the end of Adriatic Carbonate Platform existence, i.e., after the regional emergence between the Cretaceous and the

Palaeogene [22]. Later in the Palaeogene, deposition was dominantly a result of the strong and synsedimentary tectonics. As a result, the deposition still included, in smaller basins, carbonates (mostly Eocene) and large amounts of the flysch siliciclastic deposits. During this stage, the Dinaridic Mts. were uplifted with a maximum in the Oligocene and Miocene. The thickness of flysch in Middle Dalmatia exceeds 700 m [28]. Strata strike was in NW–SE, with a dip mostly to the NE of 30°–40°.
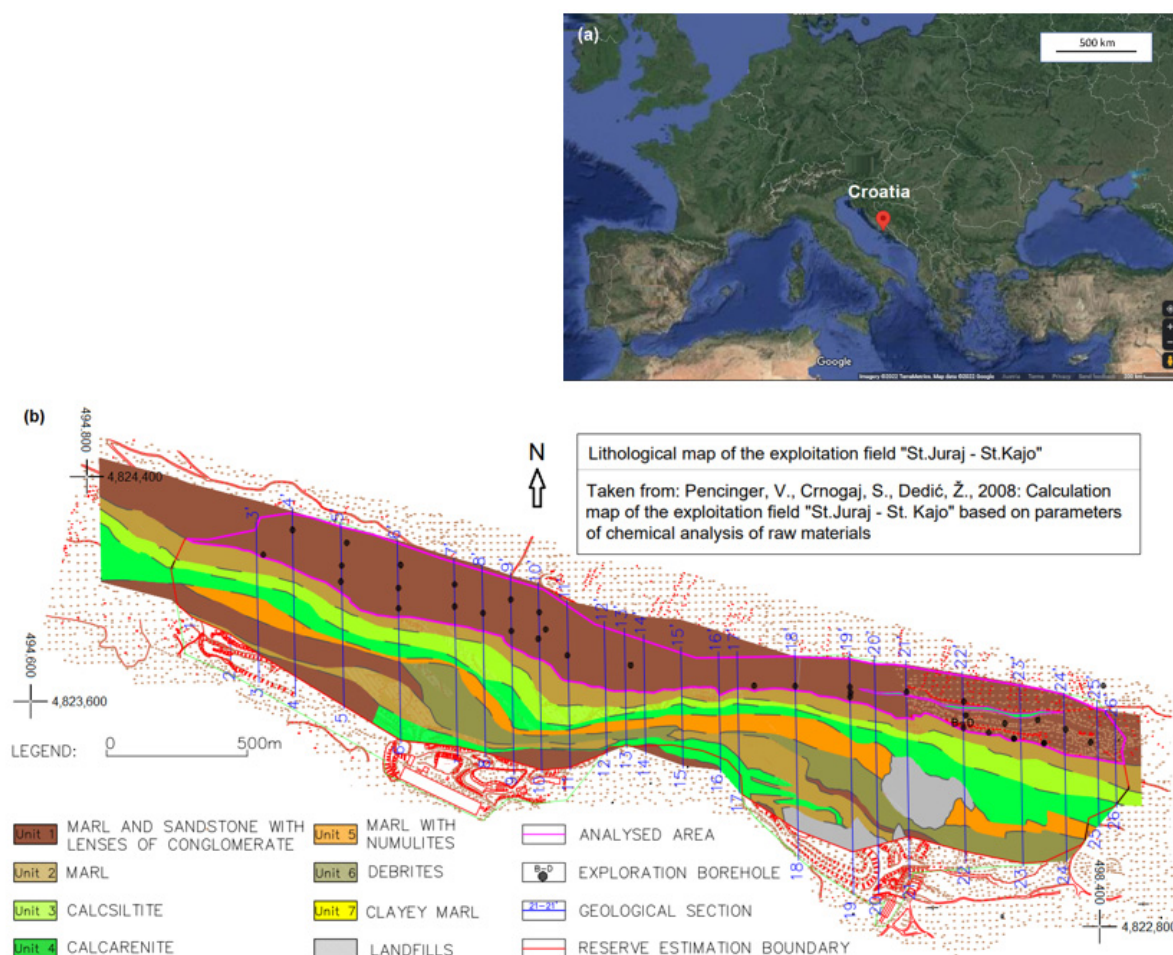

Figure 1. (**a**) Geographical location [24] and (**b**) lithological map of the exploitation field "St. Juraj–St. Kajo" (after [23,25]).

2.2. Local Lithological Units

In the exploitation field "St. Juraj–St. Kajo" there are seven different lithological units [23,25] sorted as depositional sequences. They can be divided based on $CaCO_3$ content variations after [29]:

(a)   unit 1—marl and sandstone with lenses of conglomerate; 55–70% $CaCO_3$;
(b)   unit 2—limy (calcitic) marl; 65–77% $CaCO_3$;
(c)   unit 3—clacisiltite (or clayey limestone); 77–95% $CaCO_3$;
(d)   unit 4—calcarenite (limestone); 80–95% $CaCO_3$;
(e)   unit 5—nummulite marl; 77–80% $CaCO_3$;
(f)   unit 6—debrites; 55–95% $CaCO_3$;
(g)   unit 7—clayey marl; 65–74% $CaCO_3$.

The analysed lithological unit was unit 1, where carbonate detritus varied from fine to coarse-grained and was often thinly bedded. Sand can be a significant part of the marls, calcarenites, or formed thin sandstones. Other non-carbonate components, such as chert, quartz, feldspar, pyrite, glauconite, and coal, are also present but rarely in more than

30% [23]. Unit 2 had an ideal portion of clay and limestone content for use as raw cement material. It is medium to highly weathered, often forming talus. Unit 3 was a fine-grained calcisiltite and was the transitional unit between units 2 and 4. Unit 4 was the hardest unit (calcarenite) with the carbonate detritus. Unit 5 included the nummulites with large variations of quantities, which directly affect the quality. Unit 6 was the most heterogeneous unit with large clasts (olistolites of a few meters), dominantly shallow-water limestones, deep-water mudstones, marls, and sandstones. Unit 7 was deposited dominantly at the margins of the analysed area and included a significant clay portion. This unit formed thin interlayers within other units.

For operational needs to meet the requirements of quality control for cement production, all described lithological units were divided technologically based on their chemical compounds taken from exploration boreholes data (Figure 2). Chemical analyses were performed at each 2-m depth borehole interval.
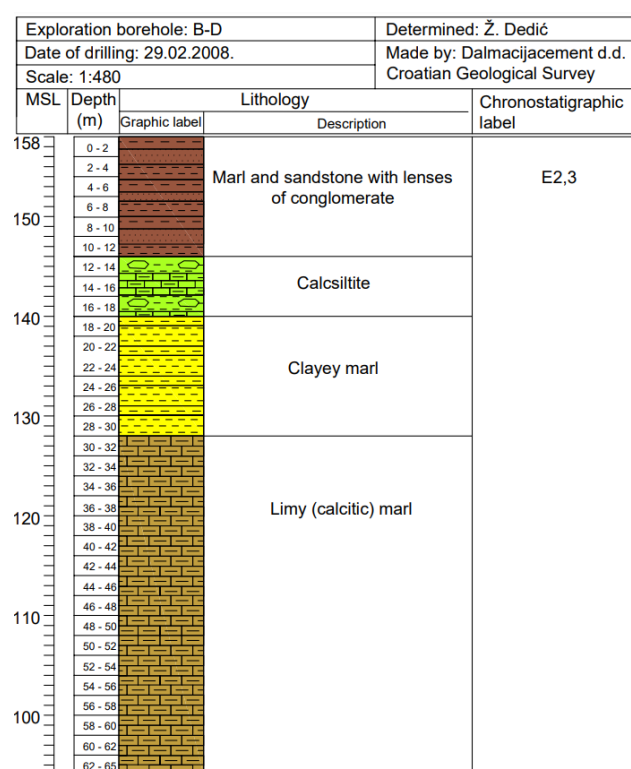

Figure 2. Exploration borehole B–D (according to [23]).

Four main oxides (CaO, SiO_2, Al_2O_3, Fe_2O_3) were used as ranking parameters, e. g., the weighting ratios of mentioned oxides define three cement modules: lime saturation factor (LSF) (Equation (1)), silicate module (SM) (Equation (2)), and aluminate module (AM) (Equation (3)) [30]:

$$LSF = [CaO/(2.8 \times SiO_2 + 1.18\ Al_2O_3 + 0.65\ Fe_2O_3)] \tag{1}$$

$$SM = SiO_2/(Al_2O_3 + Fe_2O_3) \tag{2}$$

$$AM = Al_2O_3/Fe_2O_3 \tag{3}$$

Based on the LSF values, lithological units were divided into three raw material types, as follows:

(1) high raw material (LSF > 110): calcarenite, calcisiltite, nummulite marl, debrites;
(2) normal raw material (LSF = 90–110): calcite marl, nummulite marl, debrites;
(3) low raw material (LSF < 90): marl/sandstone with conglomerate alterations, marl, clayey marl, debrites.

The further subdivision is done using the SM value. Due to heterogeneous lithological composition, a single unit (like unit 5 or unit 6) can belong to more raw material types. The modules shown in this paper will always be one of the milestones in future chemical analyses of the deposit as well as until now.

Although technologically considered homogeneous, unit 1 locally contains interlayers or lenses of different lithological characteristics such as limy (calcitic) marl (unit 2), clacisiltite (unit 3), and clayey marl (unit 7). These interlayers can locally decrease the quality of the raw materials. As the network of exploration boreholes is not dense enough, determining the extension and structure of such interlayers is uncertain. Generally, specifying the location of interlayers is more important than estimating their exact volume because the uniformity of the material's quality is not expected at the location.

According to chemical analysis from 35 exploration boreholes drilled in unit 1, a total of 11 interlayers were defined within. An example of interlayers of clayey marl, marl, and calcisiltite was shown in geological sections 22–22′ (Figure 3) [31].
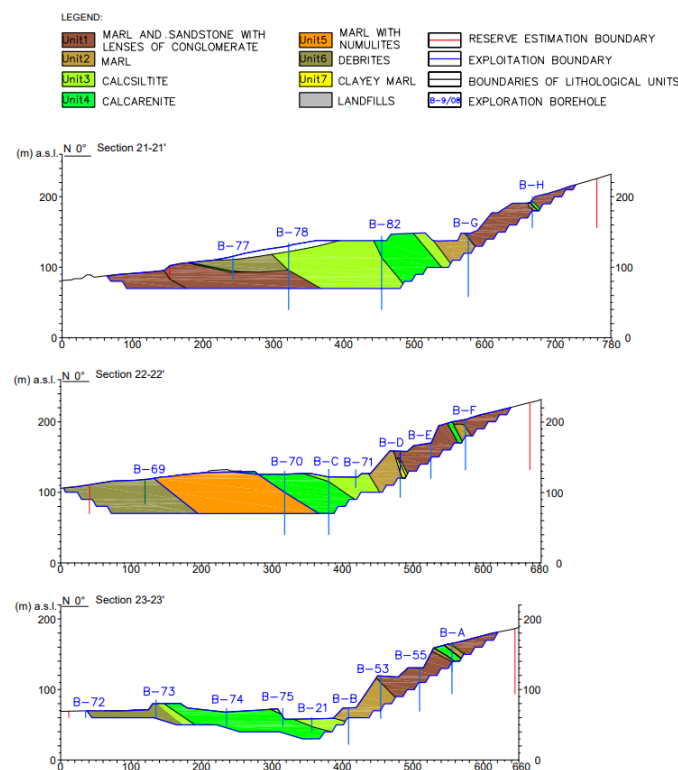

Figure 3. Geological sections 21–21′, 22–22′ and 23–23′ (according to [31]).

3. Methods

3.1. Applying Geological Sections for Volume Calculations

In the cross-section method, the reserves were performed with the calculation of the block volume (V) between two parallel vertical sections (P_1, P_2), which is obtained as a multiplication of the mean areas (P-average) of adjacent sections (P_1, P_2) multiplied by the distance between them (d). The sum of all block volumes between adjacent sections represents a particular category of reserves in the deposit. In case the areas between the adjacent sections differ by less than 50%, the volume of the block between these two sections is calculated according to [1], i.e., Equation (4):

$$V = d/2 \times (P_1 + P_2) \tag{4}$$

where are: V—block volume (m^3); P_1, P_2—section area (m^2); D—distance between sections (m).

In case the area between sections differs by more than 50%, the volume of the block between the two sections is calculated according to Equation (5) [1]:

$$V = d/3 \times (P_1 + P_2 + \sqrt{P_1 \times P_2}) \tag{5}$$

Volume calculation using geological sections was briefly described in Figure 4. There are four main vertical sections (1–1'; 2–2'; 3–3'; 4–4') at equal distances ($d_{1,2}$; $d_{2,3}$; $d_{3,4}$) and three auxiliary vertical sections (A–A'; B–B'; C–C') at half of the distance between main sections (d_A; d_B; d_C). Grey, red, and green colours indicate the borders of the geometric bodies, i.e., the theoretical case with three different types of reserve where volumes were calculated. The grey body intersects the main sections with its surfaces (P_1; P_2; P_3; P_4). The total volume of the grey body (Equation (6)) is the sum of three volumes: one on the distance $d_{2,3}$ according to Equation (4) and two on the distances $d_{1,2}$ and $d_{3,4}$ according to Equation (5). Red and green bodies are inside the grey body and represent the interlayers. The difference between the red body and the green body is that the red body is elongated over two main sections (P_5; P_6) while the green body intersects one main section (P_7). Both cases (red and green) show a significantly lower number of data than the grey case, and consequently, uncertainty is larger. In such cases, where the right extensions of strata cannot be determined, the assumption that their margins are at half the distance to the next section is applied. It means that on the auxiliary section, its area (P_A; P_B; P_C) is equal to zero. As the grey body is the largest, there are no additional, on its margins cannot be applied the rule of wedging like for green and red volumes.
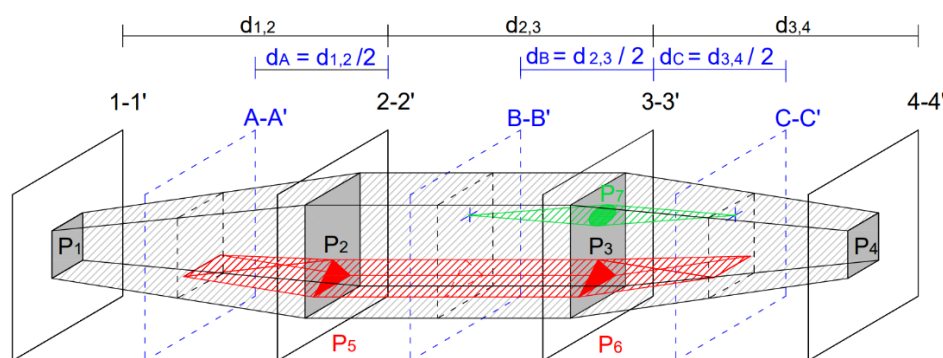

Figure 4. Sketch for volume calculation principle using geological sections.

The total volume of the red body (Equation (7)) is the sum of three volumes: one on the distance $d_{2,3}$ according to Equation (4) and two on the distances d_A and d_C according to Equation (5). The total volume of the green body (Equation (8)) is the sum of two volumes on the distance d_B and d_C according to Equation (5). Since there are red and green inside the grey body, the volume of the red and green body is subtracted from it which represents the total volume of the grey body.

$$V \text{ (grey)} = ((P_1 + P_2 + (P_1 \times P_2)^{1/2}/3 \times d_{1,2}) + ((P_2 + P_3)/2 \times d_{2,3}) + ((P_3 + P_4 + (P_3 \times P_4)^{1/2})/3 \times d_{3,4}) \text{ (m}^3) \tag{6}$$

$$V \text{ (red)} = ((P_5 + P_A + (P_5 \times P_A)^{1/2}/3 \times d_A) + ((P_5 + P_6)/2 \times d_{2,3}) + ((P_6 + P_C + (P_6 \times P_C)^{1/2})/3 \times d_C) \text{ (m}^3) \tag{7}$$

$$V \text{ (green)} = ((P_7 + P_8 + (P_7 \times P_8)^{1/2}/3 \times d_B) + ((P_7 + P_C + (P_7 \times P_C)^{1/2})/3 \times d_C) \text{ (m}^3) \tag{8}$$

3.2. Using Thickness between Structural Maps for Volume Calculation

Mathematically, the volume below some area expressed with a map can be calculated as the sum of finite volumes of observed objects "A" under the function $f(x, y)$ defined by a double definite integral (Equation (9)):

$$\text{Volume} = \int_{x_{min}}^{x_{max}} \int_{y_{min}}^{y_{max}} f(x, y) dx \, dy \tag{9}$$

Rules for integrating a function *f (x, y)* between a lower limit (x_{min}; y_{min}) and an upper limit (x_{max}; y_{max}), over a particular number of intervals, are based on numerical formulas for equally spaced lags (h) (Figure 5). As the number of intervals increases, rules for polynomials of high order are used. The range interval range is denoted by a (x_{min}) and b (x_{max}).
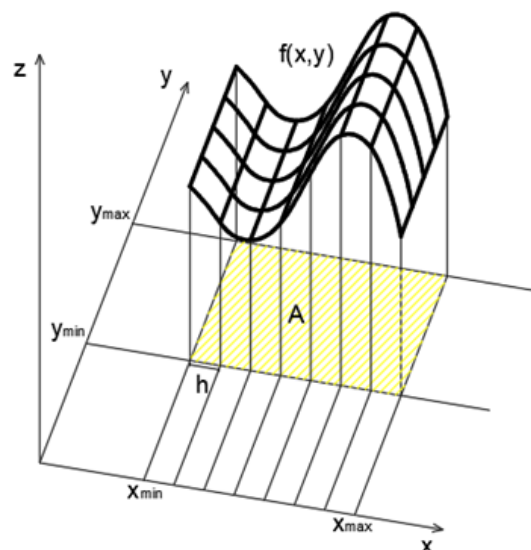

Figure 5. Equally spaced lags on the abscissa compute the definite integral of a function f(x, y).

The approximation of definite integral is obtained using three numerical integration formulas: extended trapezoidal rule (Equation (10)), extended Simpson's rule (Equation (11)) and extended Simpson's 3/8 rule (Equation (12)):

$$\int_{x_1}^{x_N} f(x)\, dx = h \left[\frac{1}{2}f_1 + f_2 + f_3 + \ldots + f_{N-1} + \frac{1}{2}f_N \right] + O \left(\frac{(b-a)^3 f''}{N2} \right) \tag{10}$$

$$\int_{x_1}^{x_N} f(x)\, dx = h \left[\frac{1}{3}f_1 + \frac{4}{3}f_2 + \frac{2}{3}f_3 + \frac{4}{3}f_4 + \ldots + \frac{2}{3}f_{N-2} + \frac{4}{3}f_{N-1} + \frac{1}{3}f_N) \right] + O \left(\frac{1}{N^4} \right) \tag{11}$$

$$\int_{x_1}^{x_N} f(x)\, dx = h \left[\frac{3}{3}f_1 + \frac{7}{6}f_2 + \frac{23}{24}f_3 + f_4 + f_5 + \ldots + f_{N-4} + f_{N-3} + \frac{23}{24}f_{N-2} + \frac{7}{6}f_{N-1} + \frac{3}{8}f_N \right] + O \left(\frac{1}{N^4} \right) \tag{12}$$

The error *(O)* for the trapezoidal rule is estimated as a product of the interval b–a divided by the number of points N (h = b–a/N) and the function's second derivation, which means the error depends on h^2. This rule gives the exact result for polynomials of degree 1. The error for more advancing Simpson's rule depends on h^4, which means the rule gives the exact result when applied to polynomials of a degree less than or equal to 3 [32].

The volume calculations by the three different formulas, Equations (10)–(12), measure the accuracy of the calculations [33]. The final volume of the observed object was reported as the average of the three values.

4. Results of the Reserve's Calculations

Based on Figure 4, the grey body refers to the unit 1 and red and green bodies exhibit the interlayers. The results of calculating the reserves using the geological section approach for unit 1 is shown in Table 1. The calculation procedure is described as below:

1. Preparing 24 geological sections used from the previous investigations [31] (from 3–3′ to 26–26′) on which are determined interlayers; eight of them are tiny and could be equivalent to the green body and three are equal in size as the red body (Figure 4). The sections used exploration boreholes located directly at the section or projected

perpendicular in the lateral plane from the "arbitrarily closest neighbourhood". Such boreholes are considered as the "hard data";

2. Determining the area (m²) of the unit 1 as well as for interlayers from each geological section (P) (Figure 3);
3. Determining the distance between the main and auxiliary sections (d) from the geological map (Figure 1);
4. Calculating the volume of the unit 1 (Vunit) according to Equations (4) and (5);
5. Calculating the volume of interlayers (Vinterlayers) according to Equations (7) and (8);
6. For each geological section where it is necessary subtract the value calculated in step 5 from the value calculated in step 4.

Table 1. Reserve of the unit 1 calculated using geological sections.

Section	Unit 1				Interlayers			
	Parea (m²)	Paverage (m²)	Distance between Main Sections (m)	Volume between Sections V = Paverage × d (m³)	Parea (m²)	Paverage (m²)	Distance between Auxiliary Sections (m)	Volume between Sections V = Paverage × d (m³)
3–3′	574							
		825	131	108,228				
4–4′	1104							
		1232	171	209,860		15.83	86	1356
5–5′	1361				47.48			
		1830	200	364,034		21.49	100	2150
6–6′	2343				17.00			
		2029	200	405,248		5.67	100	567
7–7′	1714							
		1837	100	183,635				
8–8′	1960							
		1941	100	194,049				
9–9′	1922							
		2177	99	215,215				
10–10′	2432							
		2646	101	267,596				
11–11′	2860							
		3570	131	467,207				
12–12′	4280							
		3772	71	267,971				
13–13′	3263							
		2806	68	190,090				
14–14′	2348							
		1975	132	259,998				
15–15′	1602							
		1438	133	191,888				
16–16′	1274							
		1135	66	75,238				
17–17′	996							
		1090	205	220,374		26.79	102	2742
18–18′	1183				80.38			
		1706	194	327,626		26.79	97	2592
19–19′	2289							
		2363	90	212,522				
20–20′	2437							
		2776	111	306,424		20.67	55	1145
21–21′	3114				62.00			
		3571	200	695,907		190.89	100	19,112
22–22′	4027				510.68			
		3827	204	717,671		609.40	102	62,077
23–23′	3627				355.56			
		3603	155	538,077		282.77	78	21,980
24–24′	3578				119.68			
		3032	117	348,121		118.62	59	6946
25–25′	2486				49.49			
		910	63	56,973		16.50	32	521
26–26′	20							
		Σ		6,823,952				121,188

The volume of unit 1 based on geological sections was 6,823,952 m^3 while the volume of the interlayers was 121,188 m^3 (Table 1). So, interlayers occupy a total of 2% of gross volume.
Steps in the procedure for the volume calculation by structural maps:

1. Preparing data from 35 exploration boreholes [23] from which are determined the coordinates (x, y, z) of the units 1 top and bottom, as well as of interlayers (e.g., Figure 2);
2. Interpolating top and bottom structural maps using the Ordinary Kriging (OK) with the following values:
    a. The experimental variogram for the top surface was calculated using the nugget C = 0, sills 400, range a = 240 m, total calculation distance h = 1033 m, number of classes 15, and tolerance 45°. Variogram defined searching ellipsoid with main axis 1550 m and anisotropy factor 2 (Figure 6a).
    b. The experimental variogram for the bottom surface was calculated using the nugget C = 0, sills 520, range a = 240 m, total calculation distance h = 1033 m, number of classes 15, and tolerance 45°. Variogram defined searching ellipsoid with main axis 1550 m and anisotropy factor 4 (Figure 6b).
3. Interpolating top and bottom for interlayers using (due to a low number of data) Inverse Distance Weighting (IDW). The power exponent was 2, searching circle 335 m, and anisotropy = 1 (Figure 7).
4. Calculating the volume of unit 1 using top and bottom structural maps of unit 1 and its interlayers.
5. Processing the volumes with the Equations (10)–(12);
6. Calculating averages for Equations (10)–(12);
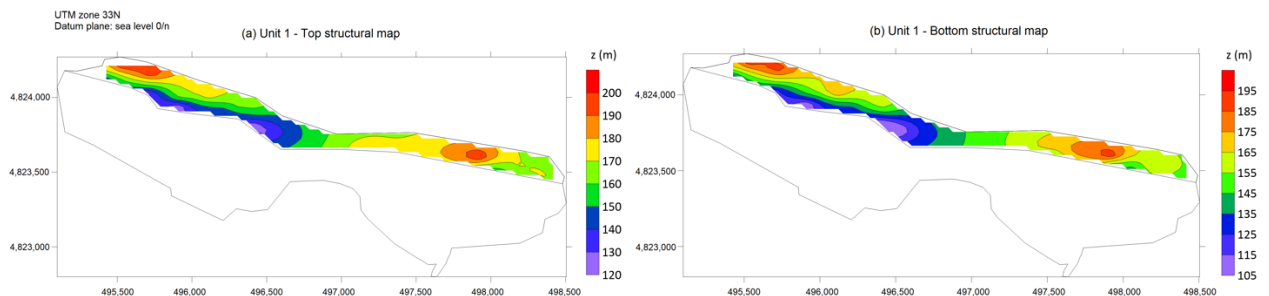7. Subtracting the volumes of interlayers from the volume of unit 1.

Figure 6. Top and bottom interpolation maps of the unit 1. (**a**): top, (**b**): bottom.
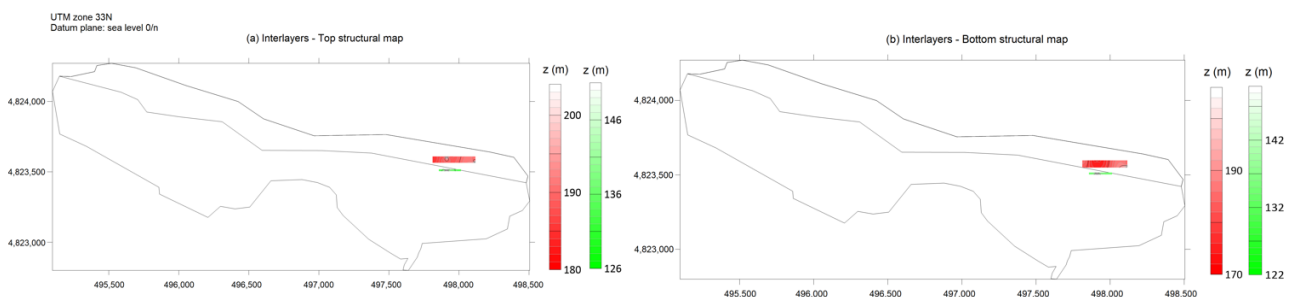

Figure 7. Top and bottom interpolation maps of the interlayers. (**a**): top, (**b**): bottom.

The volume of unit 1 calculated using structural maps was 5,808,406 m^3, while the volume of the interlayers was 276,943 m^3 (Table 2). Interlayers within unit 1 occupy a total of 5% of its volumes.

Table 2. Reserve of the unit 1 and interlayers calculated using structural maps.

	Unit 1	Interlayers
Trapezoidal Rule:	5,816,290	278,675
Simpson's Rule:	5,858,454	273,925
Simpson's 3/8 Rule:	5,750,474	278,228
Average (m^3):	**5,808,406**	**276,943**

5. Discussion

Knowledge of ore deposit geology should be considered before starting to calculate reserves. Although two approaches based on mathematical calculations of the material reserve are presented, for their interpretation, a broader geological picture should be considered. It includes the study of structures and tectonics on a local scale. In the case of mostly homogeneous deposits with similar lithologies, any approach and software will reach sufficient accurate calculation and can be performed mutually (e.g., [34]). The problem could be caused by strong tectonics, diversification of the deposits in the block, numerous depositional paleoenvironments developed over a relatively small area, and numerous lithologically different interlayers in the main units. Those all can cause high variation in grades at the low distances that should be considered.

Data taken from exploration boreholes and chemical analyses performed on cores or drilling debris are crucial for the reliability of interpretation and selection of the interpolation method. The legal regulations of mineral reserves categorization require the following certain exploration boreholes scheme. Each additional borehole must be located based on the geological situation in the deposit. Consequently, in the late exploitation phase, the number of analyses and/or boreholes is increased, as well as the accuracy of the remaining reserve calculation.

In the case of flysch deposits, which, in this research, are the raw materials for cement production, quality is extremely important. The existing network of exploration boreholes in the analysed lithological unit 1 with both approaches gave satisfactory results and an acceptable difference of 15% (Table 3). This difference represents the deviation of the calculation by the structural map method in relation to the geological section for the reserve calculation.

Table 3. Comparison of the reserves of the analysed lithological unit 1 calculated by two approaches.

Reserves of the Unit 1 (m^3)		
Geological Sections	**Structural Maps**	**Difference**
6,823,952	5,808,406	1,015,546

The calculation of the volume of very small areas, such as the example of interlayers in unit 1, is unreliable using structural mapping due to the small number of input data. The depth differences in the lenses top and bottom are very small (in the range of several meters) as opposed to in the main unit 1 (where the top and bottom can differ to a few dozen meters). Consequently, their structures are hard, clearly displaying on the same scale as the structures of the main units. It is much more difficult to assume their provision without a complete picture of the structure in which they are located, which is much easier to do on geological sections. Consequently, unit 1 interlayer's volumes, based on structural maps, were almost twice as big as the same values obtained by the geological sections approach.

6. Conclusions

In the flysch of the exploitation field "St. Juraj–St. Kajo" in the analysed lithological unit 1 that covered the largest area in the field (marl, sandstone, with lenses of conglomerates), two approaches for calculating its volume were applied; geological sections and

structural maps. The marls and sandstone of unit 1 also locally contain interlayers or lenses of different lithologies such as limy (calcitic) marl (unit 2), clacisiltite (unit 3), and clayey marl (unit 7). The importance of the interlayers is that technologically uniform material quality should not be expected at each location. In both approaches, the volume of interlayers was subtracted from the volume of unit 1.

Using geological sections for volume calculation is based on the calculation of the block volume (V) between two parallel vertical sections (P_1, P_2). Structural maps represent the calculation of the volume of the observed object under a function f (x, y) defined by a double definite integral. The volume of unit 1 calculated by the geological section method was 6,823,952 m^3, while the volume of unit 1 calculated by structural maps was 5,808,406 m^3. The difference between calculated volumes obtained by the two presented approaches was 15% which is acceptable for this research and further researchings. With more subsurface data and geological sections, the differences between the two approaches will be lesser. It is why, in the case of a very small amount of input data, e.g., in the calculation of interlayers, the method of structural maps is extremely unreliable because their spatial extension cannot assumed due to the large distance to other data, if any is available at all.

Both approaches are well-known methods. However, this is the first time that is mutually applied in the largest cement raw material facility in Croatia. It is especially important due to the production forecasts for the next decades. The trend of decreasing CO_2 emissions will probably be more rigorous in the future, which implies that reserves, especially presented with several lithotypes, will need to be predicted with less margin of errors and re-evaluated more often. Additionally, each lithological unit is characterised by its own minor (e.g., SO_3, MgO) and major oxides (CaO, SiO_2, Al_2O_3, Fe_2O_3), both important in the calculation of cement modules. That is a huge difference compared with the past when only marl had been used as raw material. Consequently, the reserve's re-evaluations would need to lead to lower error, which can be reached only if two or more methods are simultaneously applied, shown in this case.

The obtained difference suggests that the use of any method would not be inaccurate. What makes the difference is the user's need for precision. Although drawing geological sections as the method of calculating volume still ranks very high among researchers even though anyone who has encountered it knows how exhaustive and time-consuming it is. However, with a great understanding of the methods implemented in computer programs, one gains confidence in their reliability, and one should not hesitate to use them. It is also necessary to emphasise that using any Kriging technique, i.e., geostatistics in general, does not guarantee more significant accuracy at all. In the case of a small number of point data (like here for interlayers), it is impossible to calculate any reliable spatial model or prove the normal distribution of input variable(s), so the results will be uncertain and cannot be interpreted solely, without assisting of some other calculation methods. It is also a "weak point" of any complex computational algorithm, which is hardly dependent on data abundance and their regular spatial distribution.

Institutional Review Board Statement: Not applicable.

Informed Consent Statement: Not applicable.

Data Availability Statement: Not applicable.

Conflicts of Interest: The authors declare no conflict of interest.

References

1. Krklec, N.; Zidar, M. "Area"—Program for the estimation of the mineral reserves. *Rud.-Geol.-Naft. Zb.* **1989**, *1*, 35–39.
2. Peters, W.C. *Exploration and Mining Geology*, 2nd ed.; John Wiley & Sons: New York, NY, USA, 1987; 696p.
3. Al-Dabbas, M.; Awadh, S.M.; Zaid, A.A. Mineralogy, Geochemistry, and Reserve Estimation of the Euphrates Limestone for Portland Cement Industry at Al-Najaf Area, South Iraq. *Arab. J. Geosci.* **2013**, *6*, 491–503. [CrossRef]
4. Malvić, T. Stochastics—Advantages and Uncertainties for Subsurface Geological Mapping and Volumetric or Probability Calculations. *Mater. Geoenviron.* **2018**, *1*, 9–19. [CrossRef]
5. Mucsi, L.; Geiger, J.; Malvić, T. The Advantages of Using Sequential Stochastic Simulations When Mapping Small-Scale Heterogeneities of the Groundwater Level. *J. Environ. Geogr.* **2013**, *6*, 39–47. [CrossRef]
6. Zhang, J.; Srinivasan, R.S.; Peng, C. A Systematic Approach to Calculate Unit Emergy Values of Cement Manufacturing in China Using Consumption Quota of Dry and Wet Raw Materials. *Buildings* **2020**, *10*, 128. [CrossRef]
7. Habert, G.; Billard, C.; Rossi, P.; Chen, C.; Roussel, N. Cement Production Technology Improvement Compared to Factor 4 Objectives. *Cem. Concr. Res.* **2010**, *40*, 820–826. [CrossRef]
8. Chen, C.; Habert, G.; Bouzidi, Y.; Jullien, A. Environmental Impact of Cement Production: Detail of the Different Processes and Cement Plant Variability Evaluation. *J. Clean. Prod.* **2010**, *18*, 478–485. [CrossRef]
9. Imbabi, M.S.; Carrigan, C.; McKenna, S. Trends and Developments in Green Cement and Concrete Technology. *Int. J. Sustain. Built Environ.* **2012**, *1*, 194–216. [CrossRef]
10. Terzić, J.; Lukač Reberski, J. *Hydrogeological Research in the Area of the Exploitation Field "St. Juraj—St. Kayo". Fund Croatian Geological Institute 24/09—Internal Report*; Croatian Geological Survey: Zagreb, Croatia, 2009. (In Croatian)
11. Kapageridis, I.; Albanopoulos, C.; Sullivan, S.; Buchanan, G.; Gialamas, E. Application of Machine Learning to Resource Modelling of a Marble Quarry with DomainMCF. *Mater. Proc.* **2021**, *5*, 12. [CrossRef]
12. Ali, M.A.M.; Wasly, H.S.; Abdellah, W.R.; Jang, H. Optimization of blending operation for aswan phosphate mines using linear programming. *Min. Miner. Depos.* **2018**, *12*, 1–8. [CrossRef]
13. Gholamnejad, J.; Azimi, A.; Lotfian, R.; Kasmaeeyazdi, S.; Tinti, F. The application of a stockpile stochastic model into long-term open pit mine production scheduling to improve the feed grade for the processing plant. *Rud.-Geol.-Naft. Zb.* **2020**, *35*, 115–129. [CrossRef]
14. Zaki, M.M.; Chen, S.; Zhang, J.; Feng, F.; Khoreshok, A.A.; Mahdy, M.A.; Salim, K.M. A Novel Approach for Resource Estimation of Highly Skewed Gold Using Machine Learning Algorithms. *Minerals* **2022**, *12*, 900. [CrossRef]
15. Auguścik-Górajek, J.; Mucha, J.; Wasilewska-Błaszczyk, M.; Kaczmarek, W. Problems of Estimating the Resources of Accompanying Elements: A Case Study from the Cu-Ag Rudna Deposit (Legnica-Głogów Copper District, Poland). *Minerals* **2021**, *11*, 1431. [CrossRef]
16. Vu, T.; Drebenstedt, C.; Bao, T. Assessing geological uncertainty of a cement raw material deposit, southern Vietnam, based on hierarchical simulation. *Int. J. Min. Sci. Technol.* **2020**, *30*, 819–837. [CrossRef]
17. Yunsel, T.Y. Simulation of cement raw material deposits using plurigaussian technique. *Open Geosci.* **2018**, *10*, 889–901. [CrossRef]
18. Ozdemir, A.C.; Dag, A.; Ibrikci, T.A. Comparative Assessment on Cement Raw Material Quarry Quality Distribution via 3-D Identification. *J. Min. Sci.* **2018**, *54*, 609–616. [CrossRef]
19. Velić, I.; Vlahović, I.; Matičec, D. Depositional sequences and palaeogeography of the Adriatic Carbonate Platform. *Mem. Soc. Geol. Ital.* **2002**, *57*, 141–151.
20. Velić, J.; Malvić, T.; Cvetković, M.; Velić, I. Stratigraphy and petroleum geology of the Croatian part of the Adriatic Basin. *J. Pet. Geol.* **2015**, *38*, 281–300. [CrossRef]
21. Malvić, T.; Velić, J.; Cvetković, M.; Vekić, M.; Šapina, M. Određivanje novih pliocenskih, pleistocenskih i holocenskih litostratigrafskih jedinica u hrvatskom dijelu Jadrana (priobalju). *Geoadria* **2015**, *20*, 85–108. [CrossRef]
22. Vlahović, I.; Tišljar, J.; Velić, I.; Matičec, D. Evolution of the Adriatic Carbonate Platform: Palaeogeography, main events and depositional dynamics. *Palaeogeogr. Palaeoclimatol. Palaeoecol.* **2005**, *220*, 333–360. [CrossRef]
23. Pencinger, V.; Ožanić, M.; Crnogaj, S.; Dedić, Ž.; Jurić, A. *Study on the Reserves of Mineral Raw Materials for the Production of Cement in the Exploitation Field "St. Juraj—Sv. Kajo"—Restoration*; Internal Report; Croatian Geological Survey: Zagreb, Croatia, 2009. (In Croatian)
24. Google Maps. Available online: https://www.google.com/maps/place/21000,+Split,+Croatia/@49.6222155,2.4925564,3738570m/data=!3m1!1e3!4m5!3m4!1s0x13355dfc6bbcf517:0xa1798ff631b49f98!8m2!3d43.5147118!4d16.4435148?hl=en (accessed on 4 August 2022).
25. Bralić, N.; Malvić, T. Interpretation of Chemical Analyses and Cement Modules in Flysch by (Geo)Statistical Methods, Example from the Southern Croatia. *Processes* **2022**, *10*, 813. [CrossRef]

26. Pollak, D.; Buljan, R.; Toševski, A. Engineering geological and geotechnical features flysch in the area of Kaštela. *Građevinar* **2010**, *62*, 707–715.
27. Toševski, A.; Grgec, D.; Padovan, B. Some characteristics of Eoene flysch genesis, composition and weathering in Croatian coast belt. *Rud.-Geol.-Naft. Zb.* **2012**, *25*, 47–62.
28. Marinčić, S. Eocene flysch of the Adriatic belt. *Geol. Vjesn.* **1981**, *34*, 27–38. (In Croatian)
29. Matijaca, M.; Vujec, S. Statistical interpretation of raw materials for the cement industry in Split. *Rud.-Geol.-Naft. Zb.* **1990**, *2*, 75–81, (In Croatian with English abstract).
30. Duda, W.H. *Cement-Data-Book: International Process Engineering in the Cement Industry*; Bauverlag: Gütersloh, Germany, 1985.
31. Krasić, O. *Study on the Reserves of Mineral Raw Materials for the Production of Cement in the Exploitation Field "St. Juraj—Sv. Kajo"—Restoration*; Internal Report; Rudist d.o.o.: Zagreb, Croatia, 2018. (In Croatian)
32. Malvić, T.; Rajić, R.; Slavinić, P.; Novak Zelenika, K. Numerical integration in volume calculation of irregular anticlines. *Rud.-Geol.-Naft. Zb.* **2014**, *29*, 1–8.
33. Golden Software, Inc. Surfer 8 User's Guide, Contouring and 3D Surface Mapping for Scientists and Engineers. 2002. Available online: https://manualzz.com/doc/4237921/surfer-8-user-s-guide (accessed on 22 April 2022).
34. Ivšinović, J.; Malvić, T. Comparison of Mapping Efficiency for Small Datasets Using Inverse Distance Weighting vs. Moving Average, Northern Croatia Miocene Hydrocarbon Reservoir. *Geologija* **2022**, *65*, 47–57. [CrossRef]